Spin-Tensor–Momentum-Coupled Bose-Einstein Condensates

Xi-Wang Luo, Kuei Sun, and Chuanwei Zhang

Phys. Rev. Lett. **119**, 193001 — Published 6 November 2017

DOI: 10.1103/PhysRevLett.119.193001

Spin-tensor–momentum-coupled Bose-Einstein condensates

Xi-Wang Luo, Kuei Sun, and Chuanwei Zhang*
Department of Physics, The University of Texas at Dallas, Richardson, Texas 75080-3021, USA

The recent experimental realization of spin-orbit coupling for ultracold atomic gases provides a powerful platform for exploring many interesting quantum phenomena. In these studies, spin represents spin vector (spin-1/2 or spin-1) and orbit represents linear momentum. Here we propose a scheme to realize a new type of spin-tensor–momentum coupling (STMC) in spin-1 ultracold atomic gases. We study the ground state properties of interacting Bose-Einstein condensates (BECs) with STMC and find interesting new types of stripe superfluid phases and multicritical points for phase transitions. Furthermore, STMC makes it possible to study quantum states with dynamical stripe orders that display density modulation with a long tunable period and high visibility, paving the way for direct experimental observation of a new dynamical supersolid-like state.. Our scheme for generating STMC can be generalized to other systems and may open the door for exploring novel quantum physics and device applications.

Introduction. The coupling between matter and gauge field plays a crucial role for many fundamental quantum phenomena and practical device applications in condensed matter [1–3] and atomic physics [4]. A prominent example is the spin-orbit coupling, the coupling between a particle's spin and orbit (e.g., momentum) degrees of freedom, which is responsible for important physics such topological insulators and superconductors [2, 3]. In this context, recent experimental realization of spin-orbit coupling in ultracold atomic gases [5–13] opens a completely new avenue for investigating quantum many-body physics under gauge field [14–28].

So far in most works on spin-orbit coupling in solid state and cold atomic systems, the spin degrees of freedom are taken as rank-1 spin vectors F_i ($i = x, y, z$), such as electron spin-1/2 or pseudospins formed by atomic hyperfine states that can be large (e.g., spin-1 or 3/2). Experimentally, spin-orbit coupling for spin-1 Bose-Einstein condensates (BECs) has been realized recently [29, 30] and interesting magnetism physics has been observed [31–35]. Mathematically, it is well known that there exist not only spin vectors, but also spin tensors [e.g., irreducible rank-2 spin-quadrupole tensor $N_{ij} = (F_iF_j + F_jF_i)/2 - \delta_{ij}\mathbf{F}^2/3$] in a large spin ($\geq 1$) system. Therefore two natural questions are: *i*) Can the coupling between spin tensors of particles and their linear momenta be realized in experiments? *ii*) What new physics may emerge from such spin-tensor–momentum coupling (STMC)?

In this Letter, we address these two questions by proposing a simple experimental scheme for realizing STMC for spin-1 ultracold atomic gases. Our scheme is based on slight modification of previous experimental setup [29] and is experimentally feasible. The STMC changes the band structure dramatically, leading to interesting new physics in the presence of many-body interactions between atoms. Although both bosons and fermions can be studied, here we only consider spin-1 BECs to illustrate the effects of STMC. Our main results are:

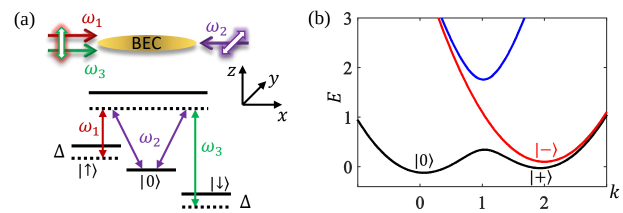

FIG. 1: (a) Top: Experimental scheme to generate STMC in BEC. Bottom: Raman transitions between three hyperfine spin states with detuning Δ. (b) Single-particle band structure for Raman strength $\Omega = 0.5$ and detuning $\Delta = 0.1$. The (dominant) spin components $|0\rangle$ and $|\pm\rangle = \frac{1}{\sqrt{2}}(|\uparrow\rangle \pm |\downarrow\rangle)$ are indicated around the corresponding band minima.

i) The single particle band structure with STMC consists of two bright-state bands (top and bottom) and one dark-state middle band [Fig. 1(b)], where the dark-state band is not coupled with two bright-state bands through Raman coupling. However, the dark-state band plays an important role on both ground-state and dynamical properties of the interacting BECs.

ii) We study the ground-state phase diagrams with exotic plane-wave and stripe phases, where the dark-state middle band can be partially populated despite not the single particle ground state. The stripe phase is a coherent superposition of two or more plane-wave states. It possesses both superfluid property as a BEC and crystal-like density modulation that spontaneously breaks translational symmetry of the Hamiltonian, satisfying two major criteria for the supersolid order [36]. Experimentally, the stripe order has recently been observed indirectly using Bragg reflection [37]. We find the transitions between different phases possess interesting multicriticality phenomena with triple, quadruple and even quintuple points.

iii) The existence of dark middle band makes it possible to study quantum states with *dynamical supersolid-like stripe orders*. In particular, we show how to dynamically generate a stripe state with a long tunable period ($\sim 5\mu$m) and high visibility ($\sim 100\%$) of density modulation, which may be directly measured in experiments (such direct measurement is still challenging for the ground-state stripe patterns due to their short period and low visibility [38]). The dynamical stripe state as a superfluid BEC, although not the ground state, does possess interesting stripe patterns that break the translational symmetry of the Hamiltonian, resembling a dynamical supersolid-like order.

The model. We consider a setup similar as that in the recent experiment [29] but with a slightly different laser configuration, as shown in Fig. 1(a), where three Raman lasers with wavenumber k_R are employed to generate STMC. The three lasers induce two Raman transitions between hyperfine spin states $|0\rangle$ and $|\uparrow(\downarrow)\rangle$, both of which have the same recoil momentum $2k_\mathrm{R}$ along the x direction. The single-particle Hamiltonian in the spin-1 basis $(|\uparrow\rangle, |0\rangle, |\downarrow\rangle)^T$ is (we set $\hbar = 1$)

$$\widetilde{H}_0 = -\frac{\nabla^2}{2m} + \Delta F_z^2 + \left(\sqrt{2}\Omega e^{i2k_\mathrm{R}x}|0\rangle\langle +| + h.c.\right), \quad (1)$$

where $F_z^2 = |\uparrow\rangle\langle\uparrow| + |\downarrow\rangle\langle\downarrow|$ is equivalent to the spin tensor N_{zz} (up to a constant), $|+\rangle \equiv \frac{1}{\sqrt{2}}(|\uparrow\rangle + |\downarrow\rangle)$, Ω is the Raman coupling strength, and Δ is the detuning for both $|\uparrow\rangle$ and $|\downarrow\rangle$ states. We see that another spin state $|-\rangle \equiv \frac{1}{\sqrt{2}}(|\uparrow\rangle - |\downarrow\rangle)$ is always an eigenstate and does not couple to $|0\rangle$ nor $|+\rangle$ through Ω, and thus is a dark state.

Since the BEC wavefunction in the y and z directions is not affected by the Raman lasers, we can consider the physics only along the x direction [33–35]. After a unitary transformation $U = \exp(-i2k_\mathrm{R}xF_z^2)$ to quasi-momentum basis, we write the Hamiltonian in energy and momentum units $\frac{k_R^2}{2m}$ and k_R, respectively, as

$$H_0 = -\partial_x^2 + (\Delta + 4 + 4i\partial_x)F_z^2 + \sqrt{2}\Omega F_x, \quad (2)$$

where Ω and Δ are dimensionless transverse-Zeeman and spin-tensor potential, respectively, and $(i\partial_x)F_z^2$ describes the coupling between spin tensor F_z^2 and the linear momentum, *i.e.*, STMC.

The single-particle Hamiltonian has three energy bands [see a typical structure in Fig. 1(b)]. The dark-state middle band always has the spin state $|-\rangle$ and spectrum $(k-2)^2 + \Delta$, which are independent of Ω. The top and bottom bright-state bands exhibit the same behavior as the known spin-orbit-coupled spin-1/2 system with spin states $|0\rangle$ and $|+\rangle$. The decoupling of the middle band is protected by the spin-tensor symmetry $[F_x^2, H_0] = 0$, under which the middle band (top and bottom bands) corresponds to $\langle F_x^2\rangle = 0$ (1). Although the single-particle ground state always selects the bottom band, the atomic interactions can break the symmetry and drastically change the BEC's ground state as well as dynamical properties by involving the middle band.

Under the Gross-Pitaevskii (GP) mean-field approximation, the energy density becomes

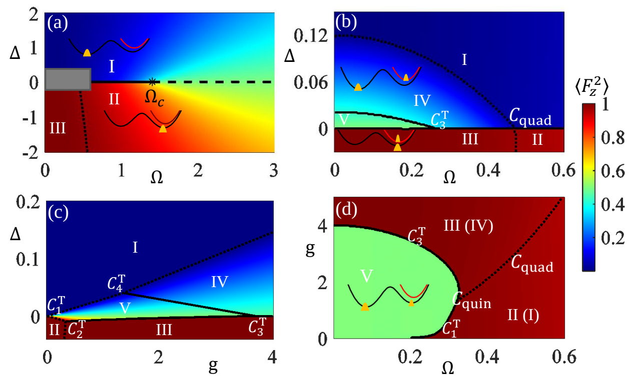

FIG. 2: (a) Ground state phase diagram in the Ω-Δ plane with $g\bar{n} = 3$. The dashed line is a crossover boundary. (b) Zoom in of the framed region in (a). (c) [(d)] Ground state phase diagram in the g-Δ (g-Ω) plane with $\Omega = 0.16$ ($\Delta = 0$). Solid (dotted) lines represent first (second) order phase transitions. The interaction ratio is $g_0 = -50g_2 \equiv g$.

$$\varepsilon = \frac{1}{V}\int dx \left[\Psi^\dagger H_0 \Psi + \frac{g_0}{2}(\Psi^\dagger\Psi)^2 + \frac{g_2}{2}(\Psi^\dagger \mathbf{F}_U \Psi)^2\right], \quad (3)$$

with V the system volume, and Ψ the three-component condensate wavefunction normalized by the average particle number density $\bar{n} = V^{-1}\int dx \Psi^\dagger\Psi$. The interaction strengths $g_{0,2}$ represent density and spin interactions in spinor condensates [39, 40], respectively. $\mathbf{F}_U = U^\dagger \mathbf{F} U$ is the unitarily transformed spin operator, whose x and y components exhibit spatial modulation that cannot be eliminated through any local spin rotation (different from previous models [33–35]). Such modulation is essential for stripe phases in the system.

We consider a variational ansatz [41]

$$\Psi = \sqrt{\bar{n}}\left(|c_1|\chi_1 e^{ik_1x} + |c_2|\chi_2 e^{ik_2x + i\alpha}\right) \quad (4)$$

to find the ground state, with $|c_1|^2 + |c_2|^2 = 1$, and spinors $\chi_j = (\cos\theta_j\cos\phi_j, -\sin\theta_j, \cos\theta_j\sin\phi_j)^T$. The energy density now becomes a functional of eight variational parameters $|c_1|$, k_1, k_2, θ_1, θ_2, ϕ_1, ϕ_2, and α, and its minimization ($\varepsilon_\mathrm{g} = \min\{\varepsilon\}$) leads to the ground state [41]. The quantum phase diagram can be characterized by the variational wavefunction, experimental observables $\langle F_z\rangle$ and $\langle F_z^2\rangle$, and the symmetry $\langle F_x^2\rangle$. The derivative of the ground-state energy $\frac{\partial\varepsilon_\mathrm{g}}{\partial\Delta} = \langle F_z^2\rangle$ ($\frac{\partial^2\varepsilon_\mathrm{g}}{\partial\Delta^2} = \frac{\partial\langle F_z^2\rangle}{\partial\Delta}$) displays discontinuity as Δ varies across a first-order (second-order) phase boundary [41]. This argument also applies to $\frac{\partial\varepsilon_\mathrm{g}}{\partial\Omega}$ ($\frac{\partial^2\varepsilon_\mathrm{g}}{\partial\Omega^2}$) [41]. We also numerically solve the GP equation using imaginary time evolution to obtain the ground states, which are in good agreement with the variational results.

Phase diagram. For ferromagnetic interaction $g_2 < 0$ (e.g., ^{87}Rb), the BEC has three plane-wave ($|c_1c_2| = 0$)

and two stripe ($|c_1c_2| \neq 0$) phases (Fig. 2): (I) plane-wave phase in $k < 1$, having $\langle F_z \rangle = 0$ (spin unpolarized), $\langle F_z^2 \rangle < 0.5$, and $\langle F_x^2 \rangle = 1$ (middle band unpopulated); (II) plane-wave phase in $k > 1$, having $\langle F_z \rangle = 0$, $\langle F_z^2 \rangle > 0.5$, and $\langle F_x^2 \rangle = 1$; (III) spin-polarized plane-wave phase in $k > 1$ having $\langle F_z \rangle \neq 0$ and $\langle F_x^2 \rangle < 1$ (middle band populated); (IV) mix-band stripe phase, having $k_1 < 1$, $k_2 > 1$, and $\langle F_x^2 \rangle < 1$; (V) bottom-band stripe phase, same as (IV) except $\langle F_x^2 \rangle = 1$. The last three phases exhibit Z_2 ferromagnetism: phases (III), (IV), and (V) all have twofold degenerate ground states with global ferromagnetic order $\pm\langle F_z \rangle \neq 0$, $\pm\langle F_y \rangle \neq 0$, and $\pm\langle F_x \rangle \neq 0$, respectively. Note that these orders are calculated in the laboratory frame (the basis of $\widetilde{H}_0$) and reflect the energetic favor by the ferromagnetic interaction. For anti-ferromagnetic interaction $g_2 > 0$ (e.g., ^{23}Na), the system has a relatively simple phase diagram containing only two plane-wave phases (I) and (II), separated by a first-order phase-boundary at $\Delta = 0$. Hereafter we focus on the ferromagnetic case.

In Fig. 2(a) we plot the phase diagram in the Ω-Δ plane. At a sufficiently large Ω, the middle band does not participate in the ground state, so the phase diagram is similar to the spin-orbit-coupled spin-1/2 system: the two plane-wave phases (I) and (II) are separated by a first-order-transition boundary (solid line along $\Delta = 0$) if $\Omega < \Omega_c$ or a crossover one (dashed line) if $\Omega > \Omega_c$. As Ω decreases, the middle band minimum gets closer to the right minimum of the bottom band [Fig. 1(b)]. If the BEC originally stays in the plane-wave phase (II) ($\Delta < 0$), it starts to partially occupy the middle band [Fig. 2(b), bottom inset], undergoing a second-order transition (dotted curve) to the polarized phase (III). From the energetic point of view, the BEC populates to a slightly higher single particle energy state to get polarized to reduce ferromagnetic interaction energy. Note that phase (III) is still a plane-wave phase since the BEC occupies both bands at the same k.

At a small Ω and $\Delta > 0$, the energy difference between the single-particle band minimum [plane wave (I)] and the other bottom-band minimum [plane wave (II)] or the middle-band minimum is comparable to the interaction energy, so the BEC may favor the co-occupation of (I) and a higher-energy local minimum as long as the total energy can be reduced more by the interaction. In Fig. 2(b), we zoom in the framed region of Fig. 2(a) and show the emergence of two stripe phases. The mix-band stripe phase (IV) is the superposition of plane wave (I) and the one around the middle-band minimum (top inset). Phase (IV) exhibits spin-density waves due to the superposition [Fig. 3(a)] and a global ferromagnetic order $\langle F_y \rangle \neq 0$ that reduces the g_2 interaction energy, compensating the higher middle-band energy. Note that phase (IV) has a uniform total density due to the orthogonality between the middle and bottom band spins, but the spin-density waves form a stripe pattern. The bottom-band

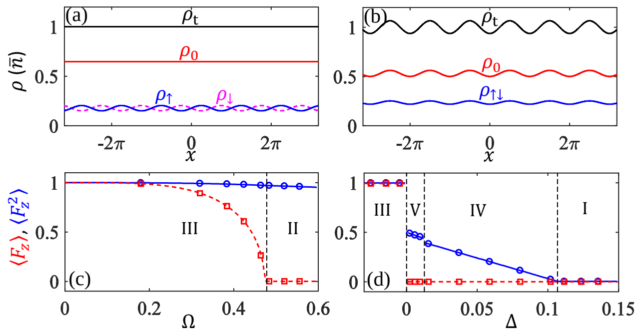

FIG. 3: (a) [(b)] The local density modulations of phase (IV) [(V)] in Fig. 2(b), with $\Omega = 0.16$ and $\Delta = 0.006$ ($\Delta = 0.023$). (c) [(d)] $\langle F_z^2 \rangle$ (blue-solid line) and $\langle F_z \rangle$ (red-dashed line) vs Ω (Δ) along the path $\Delta = -0.018$ ($\Omega = 0.16$) in Fig. 2(b). Dots (lines) are obtained from imaginary time GP equation (variational method).

stripe phase (V), which appears at even weaker Ω and Δ, is the superposition of two bottom-band plane waves (I) and (III) [Fig. 2(d) inset]. Phase (V) exhibits a total-density wave [Fig. 3(b)], which, compared with (IV), increases the g_0 interaction energy, but the total energy is favorable due to the pure bottom-band occupation and global ferromagnetic order $\langle F_x \rangle \neq 0$. We remark that the superposition of three plane waves (with co-occupation of three band minima) is never energetically favorable because it cannot maximize the ferromagnetic order.

Returning to the phase diagram Fig. 2(b), the (I)–(IV) phase boundary corresponds to a second-order transition, which meets the (II)–(III) boundary at a quadruple point $C_{\rm quad}$ at $\Delta = 0$. The (IV)–(V) boundary corresponds to a first-order transition, which encounters phase (III) at a triple point $C_3^{\rm T}$ at $\Delta = 0$. To study the dependence on interaction, we plot the phase diagram in the Δ-g plane in Fig. 2(c), with a fixed ratio $g_0 = -50g_2 \equiv g$. We see that the stripe region increases with g (due to the increasing g_2), and phase (IV) is more favorable than (V) in the large-g region (due to the large g_0). For the plane-wave phases (II) and (III), the latter has global ferromagnetic order $\langle F_z \rangle \neq 0$ and is hence favorable with strong interaction. The Δ-g diagram also shows first-order transitions between any two of (III), (IV), and (V) phases, second-order transitions between any other adjacent phases, and four triple points $C_{1,2,3,4}^{\rm T}$ at the (I)-(II)-(V), (II)-(III)-(V), (III)-(IV)-(V), and (I)-(IV)-(V) encounters, respectively. In Fig. 2(d), we show how the encounters of phases along $\Delta = 0$ change with the interaction. We see that phases (III) and (IV) survive at large g, while (I) and (II) survive at large Ω, in agreement with the energetic argument. The boundaries represent three traces of triple points $C_{1,3}^{\rm T}$ and quadruple point $C_{\rm quad}$, respectively, which intercept at a quintuple point $C_{\rm quin}$ as the joint of all five phases.

In Figs. 3(a) and (b), we plot spatial profiles of each spin component's density $\rho_{\downarrow,0,\uparrow}$ and total density ρ_t for stripe phases (IV) and (V), respectively. Phase (IV) shows out-of-phase modulations between $\rho_\uparrow$ and $\rho_\downarrow$, representing spin-vector (F_z) density wave, and uniform ρ_0 and ρ_t, while (V) shows in-phase modulations of all components and hence ρ_t, of which $\rho_{\uparrow,\downarrow}$ overlap each other, representing spin-tensor (F_z^2) density wave. The modulation wavelength matches the laser's recoil momentum $2k_R$ (i.e., $|k_2 - k_1| = 2k_R$). This can be understood in the quasi-momentum frame that the minimization of g_2 interaction requires equal modulations between the spin components and the spin operator $\mathbf{F}_U$ in Eq. (3). Since the separation between two band minima is smaller than $2k_R$ at finite Ω, the two plane-wave components of the stripe phases do not exactly stay on the band minima. In Figs. 3(c) and (d), we plot $\langle F_z \rangle$ (squares) and $\langle F_z^2 \rangle$ (circles) along (III)-(II) and (III)-(V)-(IV)-(I) transition paths in Fig. 2(b), respectively. The discontinuity in spin-tensor polarization $\langle F_z^2 \rangle$ (its first derivative) indicates the occurrence of first-order (second-order) phase transition.

Dynamical stripe state. The middle-band minimum and the right bottom-band minimum are close to each other (both near $k = 2$). Therefore a coherent superposition of plane waves on these two minima leads to a long-period stripe state, which can be directly measured in experiments. To generate such a stripe state, we consider ^{87}Rb atoms in a harmonic trap $\omega = 2\pi \times 50$Hz, initially prepared in spin state $|\uparrow\rangle$ with the Raman lasers off and $\Delta < 0$ [the initial state belongs to phase (III) since the two minima coincide and are equally populated as $|\uparrow\rangle = \frac{1}{\sqrt{2}}(|+\rangle + |-\rangle)$]. The 800-nm Raman lasers are gradually turned on such that Ω increases from 0 to Ω_f within a time T and then remains constant. If we consider an adiabatic process, where the ramping rate of Ω is much slower than the energy scale of the spin-interaction strength $g_2\bar{n}$, the system will stay in the ground-state plane-wave phase (III) until Ω exceeds the critical value where a transition to plane-wave phase (II) occurs. While for a dynamical process where the ramping rate of Ω is much faster than the spin-interaction strength (but much slower than other energy scales such as the trapping frequency), the system no longer stays in the ground state, and the BEC on the two band minima are expected to split in the momentum space, leading to the stripe state.

Figs. 4(a) and (d) show the results of real-time GP simulation for non-interacting atoms. The averaged momenta $\bar{k}_\mathrm{b}$ and $\bar{k}_\mathrm{m}$ of atoms in the bottom and middle bands follow their band minima respectively, with $\bar{k}_\mathrm{b}$ displaying slight dipole oscillation [42] at $t > T$ due to the collective excitations caused by the finite increasing rate of Ω. The final state is a stripe state similar to phase (IV) but with a much higher visibility and a longer period, and the stripe pattern is moving rather than stationary due to the dynamical phases of the two bands [41].

For atoms with realistic interactions $|g_2| \ll g_0$ and

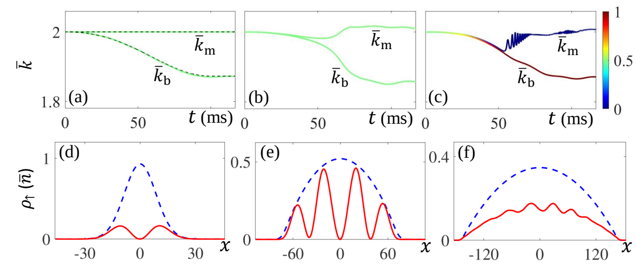

FIG. 4: (a)-(c) Averaged momentum $\bar{k}_m$ ($\bar{k}_b$) and percentage population (colorbar) of atoms in the middle (bottom) band. Thin dashed line in (a) shows the band minima. (d)-(f) The initial (dashed line) and final (solid line) spin density $\rho_\uparrow$ corresponding to (a)-(c) respectively. The interactions are $(g_0\bar{n}, g_2\bar{n}) = (0,0)$, $(0.5,0)$ and $(4,-0.2)$ for (a), (b) and (c). Other parameters are $T = 100$ms, $\Delta = -0.05$, and $\Omega_\mathrm{f} = 0.7$.

consider a dynamical process much faster compared to $g_2\bar{n}$, we can neglect the spin interaction and focus on the density-interaction effects. The density interaction preserves the symmetry F_x^2 and thus the atom populations of the two bands remain unchanged. However, $\bar{k}_\mathrm{m}$ shifts together with $\bar{k}_\mathrm{b}$ at the beginning then they separate and eventually return to their band minima respectively. At $t > T$, the density interaction induces synchronous dipole oscillations of $\bar{k}_\mathrm{m}$ and $\bar{k}_\mathrm{b}$ with a frequency different from the single-particle case [see Fig. 4(b)]. Nevertheless, we obtain a stripe state as the final state [see Fig. 4(e)] with a long period ($\sim 5\mu$m for $\Omega_\mathrm{f} = 0.7$) and high visibility (close to 100%). For ^{87}Rb with $g_2 = -0.005g_0$, such dynamical stripe states can always be obtained in the region where $|g_2|\bar{n} \ll T^{-1}$ [41]. Also, the stripe period can be tuned by changing the value of Ω_f (e.g. $\Omega_\mathrm{f} = 1$ leads to a period of $\sim 3\mu$m) [41]. Such periodic density modulations of dynamical stripe phases break the translational symmetry of the Hamiltonian, showing dynamical supersolid-like properties.

In the opposite region where the dynamical process is slow compared to the spin interaction, the system follows the plane-wave ground state. As Ω increases, atoms are transferred from the middle to bottom band until a transition to phase (II) occurs. Thus the final state has no middle-band population and no stripe states would be obtained, as shown in Figs. 4(c) and (f) with tiny stripes caused by weak excitations.

Conclusions. In summary, we propose a scheme to realize STMC in a spin-1 BEC, and study its ground-state and dynamical properties. The interplay between STMC and atomic interactions leads to many interesting quantum phases and multicritical points for phase transitions. The STMC offers a simple way to generate a new type dynamical stripe states with high visibility and long tunable periods, paving the way for direct experimental observation of long-sought stripe states. The proposed STMC for ultracold atoms open the door for exploring many other interesting physics, such as STMC fermionic superfluids, Bogoliubov excitations with interesting roton spectrum [43, 44], non-Abelian STMC (similar as Rashba spin-orbit coupling), and STMC in optical lattices (where nontrivial topological bands may emerge).

Acknowledgements: We thank P. Engels for helpful discussion. This work is supported by AFOSR (FA9550-16-1-0387), NSF (PHY-1505496), and ARO (W911NF-17-1-0128).

* Corresponding author.
Email: chuanwei.zhang@utdallas.edu

[1] D. Xiao, M.-C. Chang, and Q. Niu, Berry phase effects on electronic properties, Rev. Mod. Phys. **82**, 1959, (2010).

[2] M. Hasan and C. Kane, Colloquium: topological insulators, Rev. Mod. Phys. **82**, 3045, (2010).

[3] X.-L. Qi and S.-C. Zhang, Topological insulators and superconductors, Rev. Mod. Phys. **83**, 1057, (2011).

[4] J. Dalibard, F. Gerbier, G. Juzeliūnas, and P. Öhberg, Colloquium: Artificial gauge potentials for neutral atoms, Rev. Mod. Phys. **83**, 1523, (2011).

[5] Y.-J. Lin, K. Jiménez-García, and I. B. Spielman, Spin-orbit-coupled Bose-Einstein condensates, Nature (London) **471**, 83, (2011).

[6] J.-Y. Zhang, *et al.,* Collective dipole oscillations of a spin-orbit coupled Bose-Einstein condensate, Phys. Rev. Lett. **109**, 115301, (2012).

[7] C. Qu, C. Hamner, M. Gong, C. Zhang, and P. Engels, Observation of zitterbewegung in a spin-orbit-coupled Bose-Einstein condensate, Phys. Rev. A **88**, 021604, (2013).

[8] A. Olson, S. Wang, R. Niffenegger, C. Li, C. Greene, and Y. Chen, Tunable landau-zener transitions in a spin-orbit-coupled Bose-Einstein condensate, Phys. Rev. A **90**, 013616, (2014).

[9] P. Wang, *et al.,* Spin-orbit coupled degenerate fermi gases, Phys. Rev. Lett. **109**, 095301, (2012).

[10] L. Cheuk, A. Sommer, Z. Hadzibabic, T. Yefsah, W. Bakr, and M. Zwierlein, Spin-injection spectroscopy of a spin-orbit coupled fermi gas, Phys. Rev. Lett. **109**, 095302, (2012).

[11] R. A. Williams, M. C. Beeler, L. J. LeBlanc, K. Jiménez-García, and I. B. Spielman, Raman-Induced Interactions in a Single-Component Fermi Gas Near an s-Wave Feshbach Resonance, Phys. Rev. Lett. **111**, 095301 (2013).

[12] L. Huang, *et al.,* Experimental realization of two-dimensional synthetic spin-orbit coupling in ultracold fermi gases, Nature Phys. **12**, 540, (2016).

[13] Z. Wu, *et al.,* Realization of two-dimensional spin-orbit coupling for Bose-Einstein condensates, Science **354**, 83, (2016).

[14] T. D. Stanescu, B. Anderson, and V. Galitski, Spin-orbit coupled Bose-Einstein condensates, Phys. Rev. A **78**, 023616 (2008).

[15] C. Zhang, S. Tewari, R. Lutchyn, and S. Das Sarma, $p_x + ip_y$ superfluid from s-wave interactions of fermionic cold atoms, Phys. Rev. Lett. **101**, 160401, (2008).

[16] C. Wu, I. Mondragon-Shem, and X.-F. Zhou, Unconventional Bose-Einstein Condensations from Spin-Orbit Coupling, Chin. Phys. Lett. **28**, 097102 (2011).

[17] C. Wang, C. Gao, C. Jian, and H. Zhai, Spin-orbit coupled spinor Bose-Einstein condensates, Phys. Rev. Lett. **105**, 160403, (2010).

[18] T.-L. Ho and S. Zhang, Bose-Einstein condensates with spin-orbit interaction, Phys. Rev. Lett. **107**, 150403, (2011).

[19] Y. Li, L. Pitaevskii, and S. Stringari, Quantum tricriticality and phase transitions in spin-orbit coupled Bose-Einstein condensates, Phys. Rev. Lett. **108**, 225301, (2012).

[20] Y. Zhang, L. Mao, and C. Zhang, Mean-field dynamics of spin-orbit coupled Bose-Einstein condensates, Phys. Rev. Lett. **108**, 035302, (2012).

[21] H. Hu, B. Ramachandhran, H. Pu, and X. Liu, Spin-orbit coupled weakly interacting Bose-Einstein condensates in harmonic traps, Phys. Rev. Lett. **108**, 010402, (2012).

[22] T. Ozawa and G. Baym, Stability of ultracold atomic bose condensates with rashba spin-orbit coupling against quantum and thermal fluctuations, Phys. Rev. Lett. **109**, 025301, (2012).

[23] M. Gong, S. Tewari, and C. Zhang, BCS-BEC Crossover and Topological Phase Transition in 3D Spin-Orbit Coupled Degenerate Fermi Gases, Phys. Rev. Lett. **107**, 195303 (2011).

[24] H. Hu, L. Jiang, X.-J. Liu, and H. Pu, Probing Anisotropic Superfluidity in Atomic Fermi Gases with Rashba Spin-Orbit Coupling, Phys. Rev. Lett. **107**, 195304 (2011).

[25] Z.-Q. Yu and H. Zhai, Spin-Orbit Coupled Fermi Gases across a Feshbach Resonance, Phys. Rev. Lett. **107**, 195305 (2011).

[26] C. Qu, Z. Zheng, M. Gong, Y. Xu, L. Mao, X. Zou, G. Guo, and C. Zhang, Topological superfluids with finite-momentum pairing and Majorana fermions, Nat. Commun. **4**, 2710 (2013).

[27] W. Zhang and W. Yi, Topological Fulde-Ferrell-Larkin-Ovchinnikov states in spin–orbit-coupled Fermi gases, Nat. Commun. **4**, 2711 (2013).

[28] V. Galitski and I. B. Spielman, Spin-orbit coupling in quantum gases, Nature (London) **494**, 49, (2013).

[29] D. Campbell, R. Price, A. Putra, A. Valdés-Curiel, D. Trypogeorgos, and I. B. Spielman, Magnetic phases of spin-1 spin-orbit-coupled Bose gases, Nat. Commun. **7**, 10897 (2016).

[30] X. Luo, *et al.,* Tunable atomic spin-orbit coupling synthesized with a modulating gradient magnetic field, Sci. Rep. **6**, 18983, (2016).

[31] Z. Lan and P. Öhberg, Raman-dressed spin-1 spin-orbit-coupled quantum gas, Phys. Rev. A **89**, 023630, (2014).

[32] S. S. Natu, X. Li, and W. S. Cole, Striped ferronematic ground states in a spin-orbit-coupled $S = 1$ Bose gas, Phys. Rev. A **91**, 023608, (2015).

[33] K. Sun, C. Qu, Y. Xu, Y. Zhang, and C. Zhang, Interacting spin-orbit-coupled spin-1 Bose-Einstein condensates, Phys. Rev. A **93**, 023615, (2016).

[34] Z.-Q. Yu, Phase transitions and elementary excitations in spin-1 Bose gases with Raman-induced spin-orbit coupling, Phys. Rev. A **93**, 033648, (2016).

[35] G. Martone, F. Pepe, P. Facchi, S. Pascazio, and S. Stringari, Tricriticalities and quantum phases in spin-orbit-coupled spin-1 bose gases, Phys. Rev. Lett. **117**, 125301, (2016).

[36] Y. Pomeau and S. Rica, Dynamics of a model of super-

solid, Phys. Rev. Lett. **72**, 2426, (1994).

[37] J. Li, *et al.,* A stripe phase with supersolid properties in spin–orbit-coupled Bose–Einstein condensates, Nature (London) **543**, 91, (2017).

[38] G. Martone, Y. Li, and S. Stringari, Approach for making visible and stable stripes in a spin-orbit-coupled Bose-Einstein superfluid, Phys. Rev. A **90**, 041604(R) (2014).

[39] T.-L. Ho, Spinor bose condensates in optical traps, Phys. Rev. Lett. **81**, 742, (1998).

[40] T. Ohmi and K. Machida, Bose-Einstein condensation with internal degrees of freedom in alkali atom gases, J. Phys. Soc. Jpn. **67**, 1822 (1998).

[41] Supplementary materials, *See supplementary materials for details.*

[42] Z. Chen and H. Zhai, Collective-mode dynamics in a spin-orbit-coupled Bose-Einstein condensate, Phys. Rev. A **86**, 041604, (2012).

[43] M. Khamehchi, Y. Zhang, C. Hamner, T. Busch, and P. Engels, Measurement of collective excitations in a spin-orbit-coupled Bose-Einstein condensate, Phys. Rev. A **90**, 063624, (2014).

[44] S.-C. Ji, L. Zhang, X.-T. Xu, Z. Wu, Y. Deng, S. Chen, and J.-W. Pan, Softening of Roton and Phonon Modes in a Bose-Einstein Condensate with Spin-Orbit Coupling, Phys. Rev. Lett. **114**, 105301 (2015).